Clathrin and AP2 are required for PtdIns(4,5)P2-mediated formation of LRP6 signalosomes

Citation	Kim, Ingyu, Weijun Pan, Sara A. Jones, Youxin Zhang, Xiaowei Zhuang, and Dianqing Wu. 2013. "Clathrin and AP2 are required for PtdIns(4,5)P2-mediated formation of LRP6 signalosomes." The Journal of Cell Biology 200 (4): 419-428. doi:10.1083/jcb.201206096. http://dx.doi.org/10.1083/jcb.201206096.
Published Version	doi:10.1083/jcb.201206096
Accessed	April 17, 2018 4:29:19 PM EDT
Citable Link	http://nrs.harvard.edu/urn-3:HUL.InstRepos:11855774
Terms of Use	This article was downloaded from Harvard University's DASH repository, and is made available under the terms and conditions applicable to Other Posted Material, as set forth at http://nrs.harvard.edu/urn-3:HUL.InstRepos:dash.current.terms-of-use#LAA

(Article begins on next page)

Clathrin and AP2 are required for PtdIns(4,5)P$_2$-mediated formation of LRP6 signalosomes

Ingyu Kim,[1] Weijun Pan,[2] Sara A. Jones,[3] Youxin Zhang,[3] Xiaowei Zhuang,[3,4] and Dianqing Wu[1]

[1]Department of Pharmacology, Yale University School of Medicine, New Haven, CT 06510
[2]Institute of Health Sciences, Shanghai Institutes for Biological Sciences, Chinese Academy of Sciences/Shanghai Jiao Tong University School of Medicine, Shanghai 200025, China
[3]Department of Chemistry and Chemical Biology, and [4]Department of Physics, Howard Hughes Medical Institute, Harvard University, Cambridge, MA 02138

Canonical Wnt signaling is initiated by the binding of Wnt proteins to their receptors, low-density lipoprotein-related protein 5 and 6 (LRP5/6) and frizzled proteins, leading to phosphatidylinositol (4,5)bisphosphate (PtdIns(4,5)P$_2$) production, signalosome formation, and LRP phosphorylation. However, the mechanism by which PtdIns(4,5)P$_2$ regulates the signalosome formation remains unclear. Here we show that clathrin and adaptor protein 2 (AP2) were part of the LRP6 signalosomes. The presence of clathrin and AP2 in the LRP6 signalosomes depended on PtdIns(4,5)P$_2$, and both clathrin and AP2 were required for the formation of LRP6 signalosomes. In addition, WNT3A-induced LRP6 signalosomes were primarily localized at cell surfaces, and WNT3A did not induce marked LRP6 internalization. However, rapid PtdIns(4,5)P$_2$ hydrolysis induced artificially after WNT3A stimulation could lead to marked LRP6 internalization. Moreover, we observed WNT3A-induced LRP6 and clathrin clustering at cell surfaces using super-resolution fluorescence microscopy. Therefore, we conclude that PtdIns(4,5)P$_2$ promotes the assembly of LRP6 signalosomes via the recruitment of AP2 and clathrin and that LRP6 internalization may not be a prerequisite for Wnt signaling to β-catenin stabilization.

Introduction

The Wnt family of secretory glycoproteins plays important roles in a wide range of biological and pathophysiological processes, including embryonic development, organogenesis, tissue homeostasis, stem cell biology, and lipid and glucose metabolism. The canonical Wnt signaling pathway leads to accumulation of a multi-functional protein β-catenin. Significant progress has been made in our understanding of Wnt cross-membrane signal transduction since the initial characterization of the interaction of low-density lipoprotein-related protein 5 and 6 (LRP5/6) with Axin and importance of LRP5/6 PPPS/TP (P is proline and S/T is serine or threonine residue) motif in the interaction (Mao et al., 2001; MacDonald et al., 2009; Clevers and Nusse, 2012). LRP5 and 6 contain several PPPS/TP motifs, which are highly conserved across the species. Wnt stimulates the phosphorylation of this motif in a GSK3-dependent manner, and the phosphorylation is required for Axin binding to LRP6

I. Kim, W. Pan, and S.A. Jones contributed equally to this paper.

Correspondence to Dianqing Wu: dan.wu@yale.edu; or Weijun Pan: weijunpan@sibs.ac.cn

(MacDonald et al., 2009). Wnt also induces the phosphorylation of LRP6 at Thr-1479, which precedes the first of LRP6 PPPS/TP motif, via CK1γ (Davidson et al., 2005). In addition, LRP6 Thr-1479 phosphorylation depends on the formation of LRP6 aggregates or signalosomes, the formation of which is induced by Wnt and dependent on an intracellular Wnt signaling protein disheveled (Dvl; Bilic et al., 2007). Additionally, LRP6 primarily interacts with Axin in the signalosomes (Bilic et al., 2007).

We screened a human kinase siRNA library and identified phosphatidylinositol kinases as being important for Wnt3a-induced LRP6 phosphorylation (Pan et al., 2008). Wnt3a, via the Dvl proteins, induces the production of phosphatidylinositol (4,5)bisphosphate (PtdIns(4,5)P$_2$), which is required for Wnt3a-induced LRP6 aggregation and Axin membrane translocation. A recent report suggests that a PtdIns(4,5)P$_2$-binding protein Amer1/WTX is involved in membrane translocation of Axin (Tanneberger et al., 2011). However, the mechanism by which PtdIns(4,5)P$_2$ regulates LRP6 signalosome formation remains

unknown. In this study, we demonstrated that clathrin and adaptor protein 2 (AP2) were components of the LRP6 signalosomes, which were recruited by PtdIns(4,5)P$_2$ and required for the signalosome formation. We also found that LRP6 signalosomes were primarily localized at cell surfaces rather than being internalized.

Results and discussion

We investigated the potential role of PtdIns(4,5)P$_2$ in LRP6 signalosome formation by examining whether endocytic structural proteins are part of the LRP6 signalosomes, given PtdIns(4,5)P$_2$ has an important role in endocytosis (Di Paolo and De Camilli, 2006; Poccia and Larijani, 2009), a process also implicated in Wnt signal transduction (Blitzer and Nusse, 2006; Yamamoto et al., 2006; Cruciat et al., 2010). Sucrose gradient centrifugation of HEK293 cell lysates was performed to isolate the LRP6 signalosomes as previously described (Bilic et al., 2007; Pan et al., 2008). Four heavy fractions that contained the signalosomes and four light fractions as a control were pooled (Fig. 1 A). LRP6 from these two pools was immunoprecipitated using an LRP6 antibody. As a positive control (Bilic et al., 2007), Axin1 was detected only in the immunocomplexes from the heavy fraction pool, albeit more LRP6 protein was in the input and immunocomplex of the light fraction pool than those of the heavy pool (Fig. 1 B). Like Axin1, clathrin heavy chain (CHC), AP2 α and μ subunits were also exclusively detected in the immunocomplexes from the heavy fraction pool (Fig. 1 B). To the contrary, caveolin-1 was detected in the immunocomplexes from both heavy and light fraction pools, whereas early endosome antigen 1 (EEA1) was not detected in the heavy pool immunocomplex (Fig. 1 B). In agreement with coimmunoprecipitation of CHC or AP2 with LRP6 in the heavy fraction pool, we detected the presence of CHC and AP2μ in the heavy fractions of sucrose density gradient centrifugation (Fig. 1 C). Moreover, LRP6 and Axin1 were only detected in the immunocomplexes pulled down from the heavy fraction pool (Fig. 1 D). WNT3A induced PtdIns(4,5)P$_2$ accumulation that was primarily localized in the heavy fractions and could be rapidly diminished by rapamycin-induced recruitment of the FKBP and INPP PtdIns 5′-phosphatase fusion protein to membrane-bound FRB (Fig. S1 A; Pan et al., 2008). Elimination of PtdIns(4,5)P$_2$ also abrogated the presence of LRP6 (Pan et al., 2008) as well as CHC and AP2 in the heavy fractions (Fig. 1 C). Furthermore, LPR6 coimmunoprecipitated with CHC, AP2α, or AP2μ in a ligand-dependent manner in whole-cell extracts (Fig. S1, B and C). These interactions strengthened as the function of Wnt stimulation and were correlated with intensity of LRP6 phosphorylation (Fig. S1 B). Importantly, the interaction between CHC and LRP6 could be disrupted by PtdIns(4,5)P$_2$ hydrolysis (Fig. S1 C). These results together support a conclusion that LRP6 and endocytic structural proteins clathrin and AP2 form a complex that appears to share the characteristics of the LRP6 signalosome.

Next, we assessed the importance of clathrin and AP2 in WNT3A-induced formation of the LRP6 signalosome. Knockdown of either CHC or AP2μ (Fig. 2 A) reduced the amount of LPR6 detected in the heavy fractions of sucrose density gradient centrifugation (Fig. 2 B), suggesting that CHC and AP2 are important for the formation of the LRP6 signalosome. However, the presence of CHC in the heavy fractions was not affected by the knockdown of LRP5/6 (Fig. 2 C), even though LRP5/6 knockdown abrogated WNT3A-induced LRP6 phosphorylation (Fig. 2 A) and β-catenin accumulation (Fig. 2 D). On the other hand, knockdown of Dvl1/2/3, Fz2/4/5, or PIP5K1, which were previously shown to reduce Wnt-stimulated PtdIns(4,5)P$_2$ accumulation in HEK293 cells (Pan et al., 2008), decreased the presence of CHC in the heavy fractions (Fig. 2 C), suggesting that the presence of CHC in the heavy fraction may depend on PtdIns(4,5)P$_2$. Both AP2 α and μ subunits bind to PtdIns(4,5)$_2$, which is required for the formation clathrin-coated pits during endocytosis (Haucke, 2005; Ohno, 2006). Consistent with this knowledge, knockdown of AP2μ reduced the presence of CHC in the heavy fractions (Fig. 2 C). Therefore, we concluded that clathrin and AP2 were required for the formation of LRP6 signalosomes. Consistent with the importance of LRP6 signalosome in LRP6 phosphorylation and β-catenin stabilization, siRNA-mediated knockdown of CHC or AP2μ significantly inhibited WNT3A-induced LRP6 S1490 phosphorylation (Fig. 2 A), β-catenin accumulation (Fig. 2 D), and Wnt reporter gene activity (Fig. S1 D).

AP2, in addition to its role in PtdIns(4,5)P$_2$-dependent clathrin coat assembly, recognizes cargos through conserved sequences that include the YXXΦ (X, any amino acid; Φ, a bulky hydrophobic residue [Leu, Ile, Met, or Phe]) motif (Ohno et al., 1995; Boll et al., 1996). Examination of amino acid sequences of the intracellular domains of LRP5 and 6 revealed that LRP6 contains one and LRP5 contains three such motifs (Fig. S2, A and B). In addition, these motifs are highly conserved across species (Fig. S2, A and B). Mutating Tyr-1522, the Y residue in the LRP6 motif, disrupted the interaction of LRP6 intracellular domain with AP2 (Fig. 3 A). The AP2μ mutations (D176A,W421A) that disrupt its interaction with the YXXΦ motif also disrupted its interaction with LRP6 intracellular domain (Fig. 3 A). Together with the observation that cells expressing the mutant LRP6 (Y1522A) had reduced Wnt signaling activities (Fig. 3, B and C), we concluded that the YXXΦ motif has an important role in AP2 interaction and Wnt signal transduction.

In cells expressing exogenous LRP6, the signalosomes could be observed by confocal microscopy at the plasma membranes (Bilic et al., 2007; Pan et al., 2008). To determine how much of the endogenous LRP6 signalosomes are localized at cell surface, we used a reversible cell surface protein biotinylation approach as described in Fig. S2, C and D. We found that cell surface LRP6, rather than internalized LRP6, was detected in the heavy fractions of sucrose density gradient centrifugation (Fig. 4 A). This result suggests that LRP6 signalosomes are primarily localized at the cell surface. Next, we examined the effect of WNT3A on overall LRP6 internalization using a similar biotinylation approach, but without the step of sucrose density gradient centrifugation (Fig. S2 C), and observed no significant decreases in surface LRP6 contents or increases in internalized LRP6 contents in HEK293 cells after Wnt stimulation (Fig. 4 B and Fig. S2 E). There was a low level of constitutive LRP6
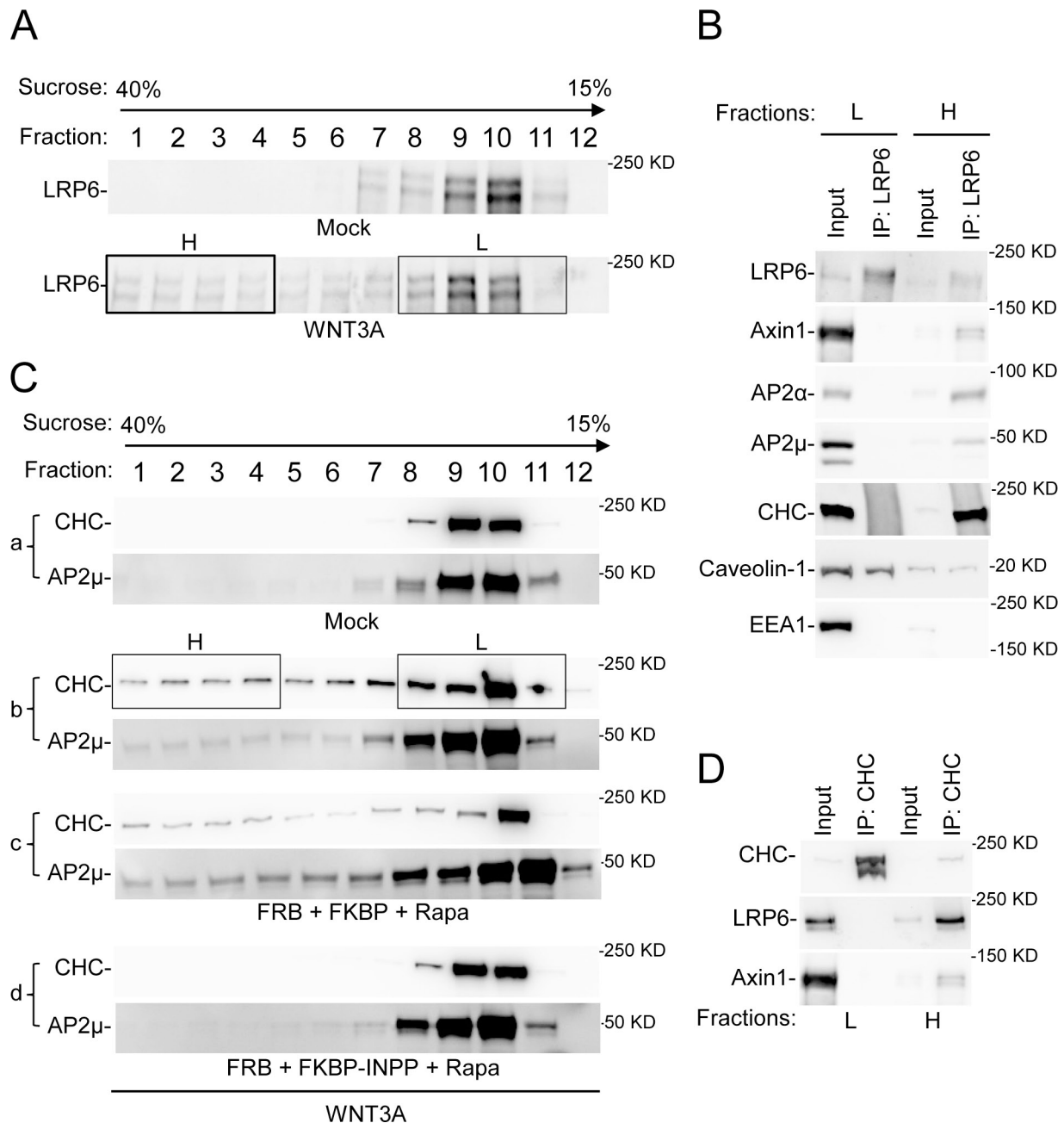
Figure 1. **Interaction of LRP6 with CHC and AP2 in its signalosome.** (A and B) CHC or AP2 interacts with the LRP6 aggregates. Cells were treated with 50 ng/ml WNT3A for 3 h, and fraction aliquots were analyzed by Western blot (A). Fractions 1–4 (H) and 8–11 (L) from the WNT3A-treated sample were pooled and subjected to immunoprecipitation (IP) by an anti-LRP6 antibody (B). Equal amounts of pooled fraction inputs were also loaded as controls. (C) WNT3A induces the co-migration of CHC and AP2 in sucrose density gradient centrifugation. HEK293 cells cotransfected with FRB and FKBP or FKBP-INPP were treated with WNT3A for 3 h as indicated. Rapa, rapamycin (100 nM). (D) LRP6 interacts with CHC aggregates. Fractions in C were pooled as indicated and subjected to immunoprecipitation using an anti-CHC antibody.

internalization, but independently of Wnt stimulation (Fig. 4 B and Fig. S2 E). In addition, the increases in the levels of phosphorylated LRP6 in whole-cell lysates or on cell surfaces could be detected even at 5 min of WNT3A treatment, but there were little increases in the phosphorylation of internalized LRP6 (Fig. 4 B). This result is consistent with the idea that LRP6 phosphorylation may primarily occur at the cell surface (some internalized phosphorylated LRP6 was detected at 3 h of WNT3A stimulation in Fig. S2 E, which may be due to the constitutive internalization). In contrast to LRP6, cell surface EGF receptors rapidly disappeared or were internalized upon EGF stimulation (Fig. S2 F). Of note, Wnt treatment did not affect EGF receptor endocytosis, nor did EGF treatment affect LRP6 endocytosis (Fig. S2 F). We also performed the biotinylation experiments in mouse embryo fibroblast (MEF) cells, and the results were the same as those in the HEK293 cells (Fig. S2 G). Thus, these data collectively indicate that LRP6 signalosomes are primarily localized at cell surfaces and that WNT3A does not induce significant LRP6 internalization in HEK293 and MEF cells.
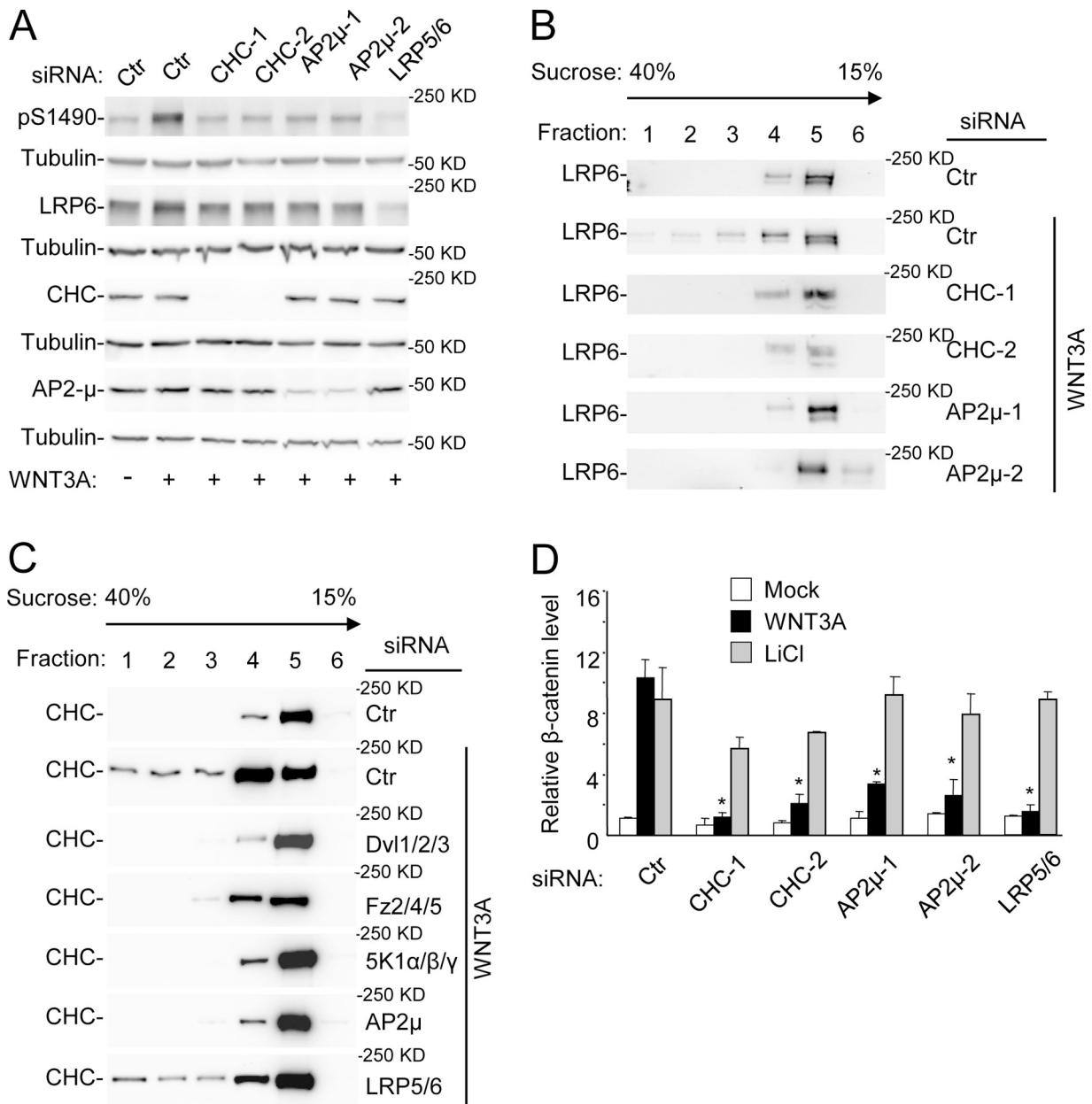
Figure 2. Requirement of clathrin and AP2 for LRP6 signalosome formation and Wnt signaling. Cells were transfected with siRNAs, treated with 50 ng/ml WNT3A for 3 h, and subjected to Western analysis (A), sucrose density gradient centrifugation (B and C), or a β-catenin ELISA (D). Ctr, control; 5K1, PIP5K1. Data in D are presented as mean ± SD (*, P < 0.01 vs. the corresponding Ctr siRNA transfection; Student's *t* test).

Knowing that PtdIns(4,5)P$_2$ hydrolysis is required for the late steps of clathrin-mediated endocytosis (Krauss and Haucke, 2007; McMahon and Boucrot, 2011), we hypothesized that the high concentrations of PtdIns(4.5)P$_2$ formed upon Wnt stimulation might prevent LRP6 from being internalized. Consistent with this hypothesis, artificial induction in PtdIns(4,5)P$_2$ hydrolysis using the rapamycin-inducible system in cells pretreated with WNT3A led to a reduction in the cell surface LRP6 (Fig. 4 C). Given that the short-term rapamycin treatment did not affect total or phosphorylated LRP6 contents in the whole-cell extracts (Fig. 4 C), we conclude that the reduction in the cell surface LRP6 by rapamycin is due to internalization.

Consistent with the biochemical evidence that WNT3A does not induce marked LRP6 internalization, WNT3A did not visibly reduce LRP6 staining at the surfaces of MEF cells examined by confocal fluorescence microscopy (Fig. 5 A). The specificity of LRP6 staining was confirmed by siRNA-mediated knockdown (Fig. 5 A and Fig. S3 A). In addition, Wnt treatment increased apparent cell surface CHC staining compared with mock or serum treatment (Fig. 5 B). We used one of the super-resolution fluorescence microscopic techniques, stochastic optical reconstruction microscopy (STORM; Rust et al., 2006; Huang et al., 2008b), to gain a higher resolution view of the staining at cells surfaces. Given the thickness
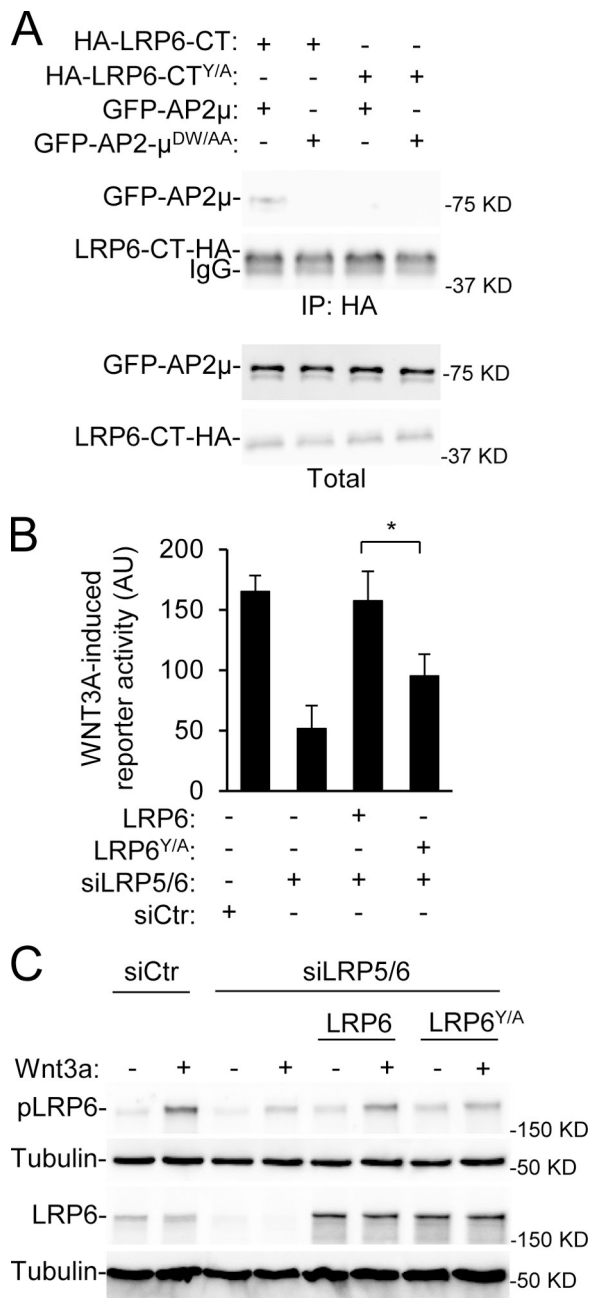
Figure 3. **Role of Tyr-1522 in Wnt signaling.** (A) The interaction of LRP6 C terminus with AP2μ depends on the YXXΦ motif. Cells were transfected with plasmids encoding LRP6 intracellular domain (CT), AP2μ, or their mutants as indicated. Immunoprecipitation was performed 24 h after transfection. (B and C) LRP6 Tyr-1522 is important for Wnt signal transduction. HEK293 cells were transfected with control (siCtr) or LRP5/6 siRNAs (siLRP5/6), followed with transfection with LRP6 and Wnt reporter gene plasmids. Data in B are presented as means ± SD (*, P < 0.05; Student's t test).

of MEF cells and the relatively high nonspecific fluorescence background signal, we focused on the bottom surfaces that are more proximal to the objective. WNT3A induced appreciable clustering of LRP6 (Fig. 5, C and D) and significant cluster size distribution shift toward larger size clusters upon Wnt treatment (Fig. S3 B). Knockdown of LRP6 significantly reduced the number of LRP6 clusters (Fig. 5, C and D; and Fig. S3, A and B).

In serum-starved or -treated MEFs stained for clathrin, STORM revealed numerous clathrin patches with morphology and sizes (100–200 nm) consistent with those of endocytic clathrin-coated pits (Fig. 5, E and F). There were also a small number of larger patches of clathrin staining (>200 nm), which may be the previously described clathrin-coated plaques (Kirchhausen, 2009). WNT3A treatment significantly increased the number of clathrin plaques, especially those with sizes greater than 400 nm (Fig. 5, E and F; and Fig. S3 C). Knockdown of AP2μ reduced the numbers of the large LRP6 clusters and clathrin plaques (Fig. S3, D–H), which is consistent with the important roles of AP2 in the formation of clathrin-coated structures and LRP6 signalosomes. Moreover, in agreement with the results of sucrose density gradient centrifugation (Fig. 2 C), knockdown of LRP6 did not affect the number of the large clathrin plaques (Fig. S3, F–H). This result once again supports the conclusion that clathrin clusters form upstream and independently of LRP6 cluster formation. In addition, these results support the conclusion that WNT3A may induce the aggregation of LRP6 and clathrin at the cell surface.

Next, we wanted to image the cell surfaces exposed to the culture medium rather than those attached to the coverslip, as the attachment to the coverslip glass surface may induce artifacts. We have previously imaged through BS-C-1 cells, a monkey kidney cell line with a thinner morphology, by 3D STORM (Huang et al., 2008a). WNT3A could stimulate LRP6 phosphorylation, while not inducing marked LRP6 internalization, in these cells (Fig. S3 I). We performed 3D STORM imaging of BS-C-1 cells stained for LRP6 or clathrin. Similar to MEF cells, we observed increases in LRP6 and clathrin cluster sizes at both top and bottom surfaces of cells treated with WNT3A (Fig. 5, G–K; and Fig. S3 J). We also found that knockdown of Dvls blocked the formation of these clusters (Fig. S3 K). Using the two spectrally distinct photoswtichable dyes Alexa Fluor 647 and Atto 488 for STORM (Dempsey et al., 2011), we also performed 3D imaging of BS-C1 cells co-stained for LRP6 and clathrin light chain (CLC) and observed some colocalization of LRP6 and clathrin clusters at cell surfaces (Fig. 5 L). The fractional colocalization of LRP6 with clathrin clusters increased substantially upon Wnt stimulation, from 6% in mock-treated cells to 42% upon stimulation for LRP6 clusters greater than 100 nm in size. The change was less pronounced for the small LRP6 clusters (from 10 to 30%).

In this study, we used biochemical and imaging approaches to characterize the LRP6 signalosome. Our results suggest that clathrin and AP2 may be the structural components of the LRP6 signalosomes and recruited to form a complex by Wnt-induced PtdIns(4,5)P_2, which in turn recruits LRP6 (Fig. S3 L). Despite the fact that the formation of this signalosome does not depend on LRP6, we continue to refer the complex in this article to as "LRP6 signalosome" both for the historic reason and for the reason that the downstream signaling events tested in this study depend on LRP6 aggregation. In HEK293 cells, MEF cells, and BS-C-1 cells, the LRP6 signalosomes seem to be primarily localized at cell surfaces, and WNT3A does not strongly induce LRP6 internalization in contrast to observations made in some tumor cell lines (F9 and Hela cells) or in
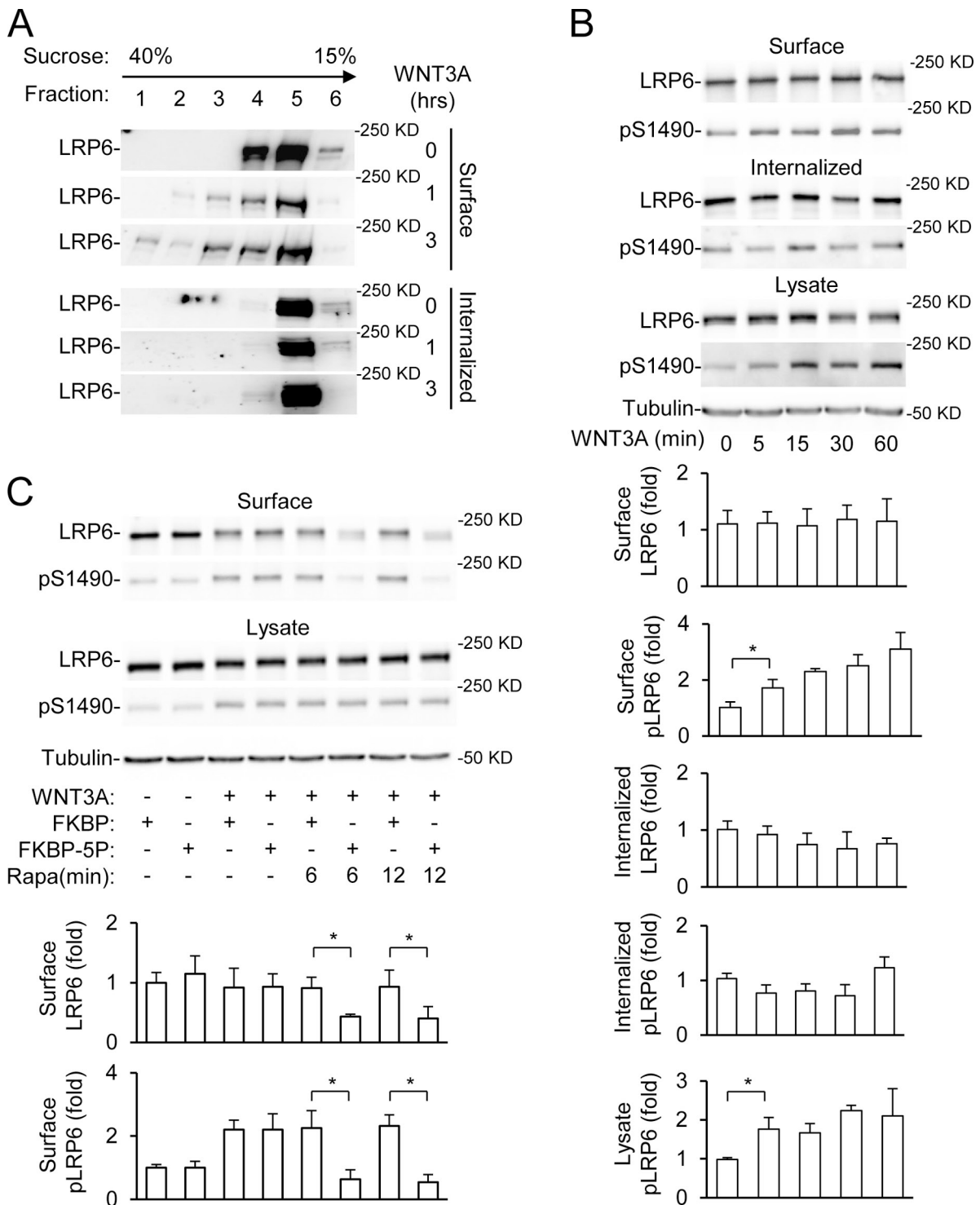
Figure 4. **WNT3A-induced LRP6 signalosomes are primarily localized at cell surfaces.** (A) LRP6 signalosomes are localized at cell surfaces. HEK293 cells were stimulated with 50 ng/ml WNT3A and labeled with biotins, followed by sucrose density gradient sedimentation. Fractions were then subjected to precipitation using NeutrAvidin beads and analyzed by Western blot. (B) WNT3A does not induce significant internalization of LRP6. HEK293 cells were stimulated with 50 ng/ml Wnt for times indicated and labeled with biotins. After precipitation using the NeutrAvidin beads, precipitated proteins and whole-cell lysates were analyzed by Western blot. (C) Forced hydrolysis of PtdIns(4,5)P_2 leads to LRP6 internalization. HEK293 cells were cotransfected with FRB and FKBP or FKBP-INPP and treated with 50 ng/ml WNT3A for 45 min followed with rapamycin treatment. Experiments in B and C were performed three times. Data are presented as means ± SD (*, P < 0.05; Student's *t* test).

cells overexpressing LRP6 (Yamamoto et al., 2006; Jiang et al., 2012; Sakane et al., 2012). This apparent discrepancy in LRP6 internalization may be due to the difference in the stoichiometry of LRP6 signalosome components among these cells. LRP6

signalosomes in overexpressed cells were previously observed at the cell surface, but a balanced coexpression of Fz, Dvl, and Axin was required (Bilic et al., 2007; Pan et al., 2008). Thus, it is possible that LRP6 that cannot be incorporated into
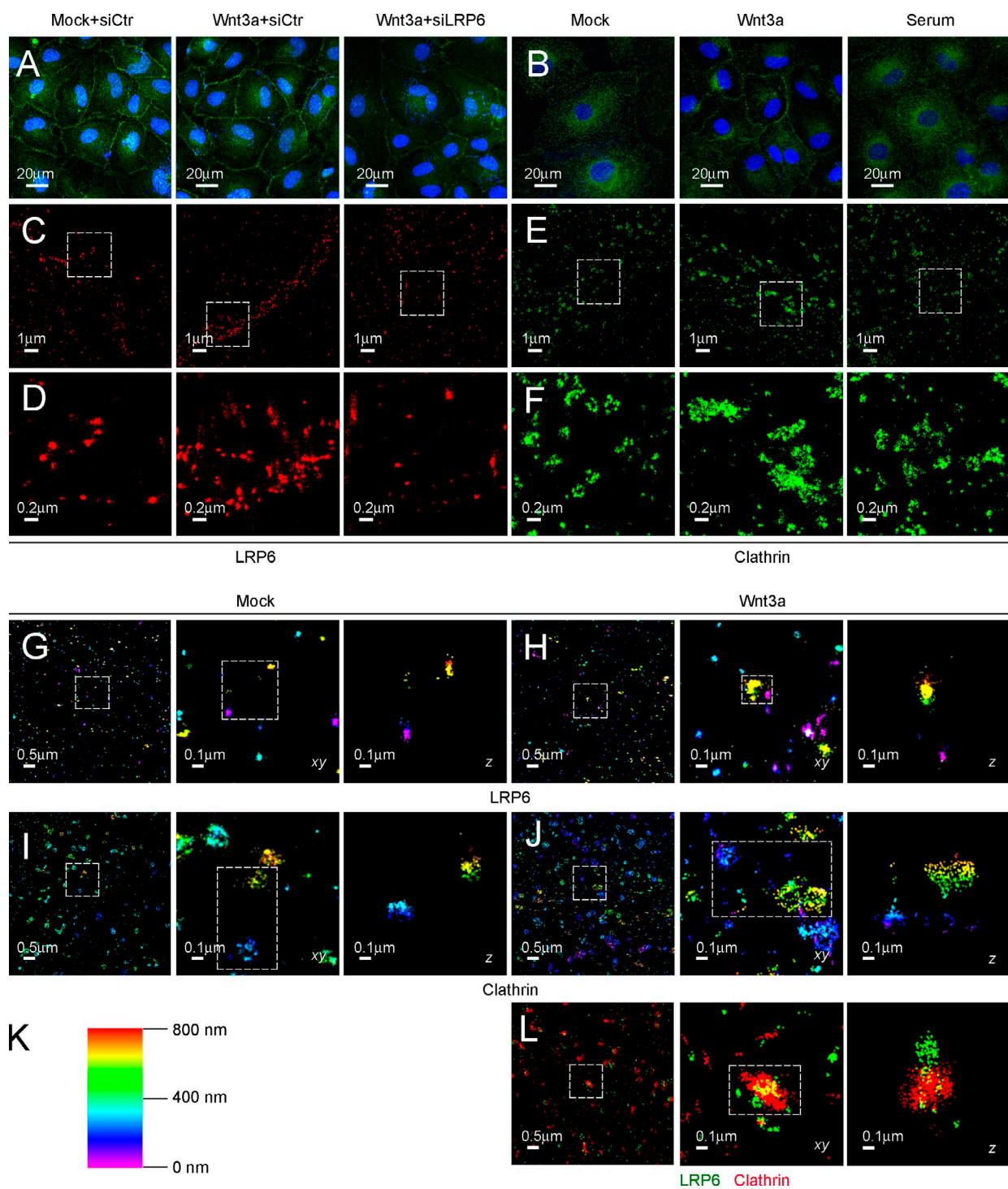
Figure 5. **Imaging of WNT3A-induced LRP6 and clathrin clusters at cell surface.** (A) WNT3A treatment does not reduce membrane localization of LRP6. MEF cells were transfected with the control siRNA (siCtr) or LRP6 siRNA (siLRP6) for 2 d followed by serum starvation overnight. The cells were then treated with mock or WNT3A (50 ng/ml, 1 h) and examined by a confocal microscope. (B) WNT3A increases membrane localization of clathrin. MEF cells were serum starved, treated with mock, WNT3A (50 ng/ml), or serum (10% FCS) for 1 h at 37°C, and examined by a confocal microscope. (C–F) WNT3A induces the formation of clathrin and LRP6 clustering at cell surfaces. MEF cells were treated as described above and analyzed by STORM. Treatment with WNT3A visibly increases the cluster size of both LRP6 (C and D) and clathrin (E and F) located on the adherent surface of the cell, as compared with control treatments. D and F are enlargements of the boxed areas in C and E, respectively. (G–K) Three-dimensional imaging of LRP6 or clathrin clustering. BS-C-1 cells were serum starved and treated with mock or WNT3A (50 ng/ml) for 1 h at 37°C. The cells were fixed, stained with anti-LRP6 or anti-CLC antibody, and analyzed by 3D STORM. The first two sub-panels are *xy* projections of the 3D dataset, with the second sub-panel being an enlargement of the boxed region in the first. The third sub-panel is the *xz* projection of the boxed region in the previous sub-panel. The *z*-dimension position information is color coded according to the color scale bar (K), with lower values being closer to the coverslip. (L) Colocalization of LRP6 and clathrin at cell surfaces. BS-C-1 cells were treated as in G and stained with anti-LRP6 and anti-CLC antibody. The cells were analyzed by 3D STORM, and a representative image is shown. The first two sub-panels are *xy* projections of the 3D dataset, with the second sub-panel being an enlargement of the boxed region in the first. The third sub-panel is the *xz* projection of the boxed region in the previous sub-panel.

the signalosomes may be internalized. The second possible explanation is the differences in the kinetics of PtdIns(4,5)P_2 metabolism among these cells, because the presence of LRP6 signalosomes on cell surfaces depends on high levels of PtdIns(4,5)P_2. Another possibility is differences in the levels of various endocytic components, which may skew LRP6 to caveolin-dependent endocytosis (Yamamoto et al., 2006; Jiang et al., 2012). Nevertheless, the failure of WNT3A to induce clear LRP6 internalization in the three cell lines we tested in this study suggests that LRP6 internalization may not be a prerequisite for Wnt signaling to β-catenin stabilization. However, our results do not exclude the possibility that vesicle transport or even endocytic vesicle transport has a role in Wnt–β-catenin signaling.

In addition to LRP5/6–AP2 interaction, Dvl also interacts with AP2 (Yu et al., 2007, 2010), which may provide another link of the signalosome to the clathrin-coated structure. It would be of interest to know whether this Dvl–AP2 interaction has a role in LRP6 signalosome formation and Wnt–β-catenin signaling, even though this link is important for noncanonical Wnt signaling. On the subject of noncanonical Wnt signaling, WNT5A, a prototypical noncanonical Wnt, can also stimulate PtdIns(4,5)P_2 formation (Grumolato et al., 2010) and Dvl aggregation (Nishita et al., 2010). These findings together raised a possibility that PtdIns(4,5)P_2 may also be involved in signalosome formation in noncanonical Wnt signaling. Thus, CHC/AP-2/PtdIns(4,5)P_2-dependent signalosomes, which may be more appropriately referred to as Wnt signalosomes, may be formed upon all types of Wnt stimulation, but the recruitment of the Wnt co-receptors to these complexes may vary depending on the nature of Wnt proteins (Nishita et al., 2010). In this regard, it is also important to determine whether Fz and Dvl as well as other signalosome components, whose number has been growing (MacDonald et al., 2009; Wu and Pan, 2010; Tanneberger et al., 2011), have a structural role in the signalosome formation and how these signalosome components are organized in the complex.

Materials and methods

Constructs, siRNAs, reagents, and antibodies
Plasmids for wild-type and mutant of AP2μ were kindly provided by V. Haucke (Freie Universität Berlin, Berlin, Germany; Krauss et al., 2006). Plasmids for FRB, FKBP12, and FKBP12-INPP were kindly provided by T. Balla (National Institute of Child Health and Human Development, NIH, Bethesda, MD; Varnai et al., 2006). Full-length LRP6 and its mutants are in AAV-CMV vector (Agilent Technologies). The siRNAs were purchased from Thermo Fisher Scientific. The siRNA sequences for Fz2/4/5, LRP5/6, PIP5K1α/1β/1γ, and Dvl1/2/3 were described previously (Pan et al., 2008). Sequences for the CHC and AP2μ siRNA are: CHC1-1, 5′-GGAAGGAAATGCAGAAGAA-3′; CHC1-2, 5′-AGAACAAGCTACAGAGACA-3′; AP2μ-1, 5′-AGGCACAGCTGAT-GAAACA-3′; and AP2μ-2, 5′-GGGCAAAGGCACAGCTGAT-3′. The control siRNA was provided by Applied Biosystems. Recombinant purified WNT3As were purchased from R&D Systems. Chemicals were purchased from Sigma-Aldrich.

Antibodies to EEA1, AP2ÿ, phosphorylated-Ser1490 LRP6, Axin1, and LRP6 (Cell Signaling Technology), caveolin-1 (BD), CHC (Abcam), and AP2α and CLC (Sigma-Aldrich) were acquired commercially. ELISA assay on free β-catenin level was performed as described previously (Pan et al., 2008).

Cell culture and immunostaining
HEK293 and MEF cells were maintained in DMEM in the presence of 10% fetal bovine serum (FBS). BS-C-1 cells were maintained in EMEM supplemented with 10% FBS. Plasmids or siRNA were transfected by Lipofectamine Plus or RNAiMAX (Invitrogen), respectively.

For immunostaining, cells were fixed in 4% paraformaldehyde for 30 min at 4°C. After permeabilization with 0.3% Triton X-100 in PBS for 5 min, the cells were blocked with 3% sheep serum, followed by primary antibodies. After washes, cells were incubated with fluorescence-conjugated secondary antibodies and were examined by a confocal microscope (model SP5; Leica) using a 60× objective. For STORM imaging, fixed cells were stained with anti-LRP6 (1:25), anti-CHC (MEF cells; 1:300), or anti-CLC (BS-C-1 cells; 1:1,000) at 4°C overnight, followed by fluorescence-conjugated secondary antibodies. Cells were imaged at room temperature (RT) in PBS supplemented with 2% glucose, 50 mM Tris, pH 8.0, an oxygen scavenging system (0.5 mg/ml glucose oxidase and 40 μg/ml catalase), and either 1% β-mercaptoethanol (single-color imaging) or 10 mM cysteamine (two-color imaging).

Immunoprecipitation
HEK293T cells were lysed with a lysis buffer containing 1% Nonidet P-40, 137 mM sodium chloride, 20 mM Tris, pH 7.4, 1 mM dithiothreitol, 10% glycerol, 10 mM sodium fluoride, 1 mM pyrophosphoric acid, 2 mM sodium vanadate, and Complete protease inhibitors (Roche). After centrifugation at 13,000 rpm for 30 min at 4°C, the supernatants were incubated with antibody and protein A/G Sepharose beads from Santa Cruz Biotechnology, Inc. for 3 h at 4°C. The immunocomplexes were then washed and subjected to Western analysis.

Wnt activity assays
Cytosol fractions for the β-catenin ELISA assays were prepared by incubating the cells in a hypotonic buffer (10 mM Hepes-KOH, pH 7.9, and 10 mM KCl) on ice for 10 min, followed by three freeze–thaw cycles. The samples were centrifuged at 13,000 rpm for 10 min, and supernatants were collected. Protein concentrations were determined using a BCA Protein Assay kit (Thermo Fisher Scientific). ELISA plates (96 well) were coated with mouse anti–β-catenin antibody (50 μl/well at 1 μg/ml in PBS; BD) overnight at 4°C. The plate was washed once with TBST and blocked with 1% BSA in TBST at RT for 30 min. 80 μl of cytosol fraction were loaded into a well, and the plate was shaken at 600 rpm for 1 h at RT. After washing, the plate was incubated with rabbit anti–β-catenin antibody (Cell Signaling Technology) for 45 min, followed by peroxidase-conjugated goat anti–rabbit antibody (Jackson ImmunoResearch Laboratories, Inc.) for 25 min. After washing three times, chemiluminescence substrate (SuperSignal West Pico; Thermo Fisher Scientific) was added, and luminescence intensity was determined by a luminometer.

For the Wnt reporter gene assay, HEK293T cells were first transfected with siRNAs using RNAiMax followed by another transfection of Wnt reporter genes and siRNAs using Lipofectamine Plus 2 d later. Luciferase assays were performed 24 h after the second transfection and 6 h after Wnt3a stimulation. Luciferase activity was normalized against the fluorescence intensity of coexpressed GFP.

Sucrose density gradient centrifugation
Sucrose gradient sedimentation was performed as described by Bilic et al. (2007). In brief, cells were harvested in Hank's balanced salt buffer on ice, pelleted, and lysed for 20 min in an extraction buffer containing 30 mM Tris, pH 7.3, 140 mM sodium chloride, 1% Triton X-100 (Sigma-Aldrich), 25 mM sodium fluoride, 3 mM sodium orthovanadate, 2 mM PMSF, 100 nM okadaic acid, and the protease inhibitor cocktail tablet (Roche). The lysate was centrifuged, and supernatant was layered on top of a 15–40% sucrose gradient made with a buffer containing 30 mM Tris, pH 7.3, 140 mM sodium chloride, 0.02% Triton X-100, 25 mM sodium fluoride, 3 mM sodium orthovanadate, and protease inhibitors. Ultracentrifugation was performed in a rotor (model SW55; Beckman Coulter) at 100,000 g for 4 h at 4°C. After centrifugation, fractions were collected from the bottom of the tube and analyzed by Western blotting and lipid assays.

PtdIns(4,5)P_2 determination
The PtdIns(4,5)P_2 ELISA was performed as previously described with some modifications (Irie et al., 2005). Lipid extracts were dissolved directly in ethanol at RT, loaded into a microplate, and dried under vacuum. The microplate was incubated with 2% BSA in PBS (blocking buffer) at RT for 30 min, followed by mouse anti-PtdIns(4,5)P_2 monoclonal antibody (Assay Designs) for 1 h and goat anti–mouse IgG-HRP (Santa Cruz Biotechnology, Inc.) for 25 min. The microplate was washed three times with PBS after each incubation. Finally, chemiluminescence substrate (SuperSignal West Pico; Thermo Fisher Scientific) was added to the plate and luminescence intensity was determined by a luminometer.

STORM image acquisition and analysis
STORM images were acquired using an inverted optical microscope (model IX71; Olympus) equipped with three individually controlled laser

beams (657 nm [RCL-300-656; Crystalaser], 488 nm [Sapphire 488 LP-200; Coherent], and 405 nm [CUBE 405-50C; Coherent]), a 100× UPlanSApo objective (NA 1.4; Olympus), and a back-illuminated EMCCD camera (iXON DU-897; Andor Technology). The focus was maintained during data acquisition using an 830-nm fiber-coupled diode laser (LPS-830-FC; Thorlabs), detected by a quadrant photodiode, in a separate objective-type TIRF path. Acquisition was controlled using software custom written in Python.

For single-color imaging, the secondary antibodies were conjugated with Alexa Fluor 405 and 647. The probes were activated by the 405-nm laser and subsequently imaged with the Alexa Fluor 647 laser. During imaging we used an oblique-incidence imaging geometry to reduce background fluorescence while maintaining a large imaging depth (Huang et al., 2008a). The excitation beams were reflected by a dichroic longpass mirror (T660LPXR; Chroma Technology Corp.) and the fluorescence emission was filtered with a bandpass filter (ET705/72m; Chroma Technology Corp.). For two-color imaging, secondary antibodies conjugated with Alexa Fluor 647 or Atto 488 were activated by the 405-nm beam and imaged using 488- and 657-nm beams. These beams were reflected by a custom-designed polychroic mirror (ZT405/488/561/640rpc; Chroma Technology Corp.). Fluorescence emissions from Alexa Fluor 647 and Atto 488 were separated by a 630-nm longpass dichroic mounted on a commercial beamsplitting device (Dual-View; Photometrics). The short-wavelength channel was filtered with a bandpass filter (ET535/50m; Chroma Technology Corp.) for Atto 488. The long-wavelength channel was filtered with a bandpass filter (ET705/72m; Chroma Technology Corp.) for Alexa Fluor 647. In addition to the bandpass filters, a double-notch filter (NF01-488/647; Semrock) was added before the Dual-View to block the two excitation beams. The two-color channels were collected sequentially, first Alexa Fluor 647 and then Atto 488, to minimize photobleaching. Each channel was imaged onto 256 × 256 pixels of the EMCCD camera running at 60 Hz. For 3D localization, a cylindrical lens with a focal length of 100 cm was inserted into the imaging optical path (Huang et al., 2008b).

STORM images were analyzed and reconstructed using custom-written analysis software in C++ (Huang et al., 2008b). In brief, the fluorescent peaks corresponding to individual molecules were identified in each imaging frame and fit to an elliptical Gaussian to determine their lateral position (x_0 and y_0) and corresponding Gaussian widths (d_x and d_y). The widths were compared with a calibration curve, generated separately by scanning 100-nm Tetraspeck beads (Invitrogen) in the z direction, and used to determinate the axial (z) position of each molecule (Huang et al., 2008b). Molecules on in successive frames that were separated by <167 nm (1 pixel) were linked together, and the mean position of the molecule during those frames reported. The z position was also subsequently corrected to account for the refractive index mismatch between the glass and imaging medium (Huang et al., 2008a). Sample drift in the lateral and axial dimensions was corrected computationally using the correlation function of the image itself (Huang et al., 2008b). For image rendering each individual localization was plotted as a Gaussian with sigma 5–7 nm. For two-color imaging of Alexa Fluor 647 and Atto 488, the analyzed STORM images were aligned by a third-order polynomial warping map in 3D obtained from more than 40 calibration images of 100-nm Tetraspeck fluorescent beads taken across the imaging volume (Jones et al., 2011). The residual alignment error was ∼9–12 nm in the lateral dimensions and ∼18 nm in the axial dimension.

For cluster analysis, STORM images were subjected to a density-based clustering of applications with noise (DBSCAN) cluster algorithm. For MEFs, areas were randomly selected for the analysis. For BS-C-1 cells, cluster analysis was limited to a thin ∼10 × 13 µm (60 × 80 pixel) region of the cell containing both top and bottom cell surfaces (based on the 3D analysis). For the DBSCAN analysis, epsilon values of either 100 or 60 and n values of 50 or 45 were used for clathrin or LRP6 images, respectively. For size measurements, clusters were modeled as circular, and all sizes are reported in diameter.

Cell surface protein biotinylation
The reversible cell surface protein biotinylation was performed as described previously (Nishimura and Sasaki, 2008; Semënov et al., 2008; Sakane et al., 2010) with some modifications. For detection of cell surface LRP6, cell surface proteins were biotinylated with 0.5 mg/ml of EZ-Link Sulfo-NHS-SS-Biotin (Thermo Fisher Scientific) in a PBS buffer on ice and were washed with PBS containing 50 mM NH_4Cl on ice. Cells were then washed with PBS and lysed in a lysis buffer (1.25% Triton X-100, 0.25% SDS, 50 mM Tris HCl, pH 8.0, 150 mM NaCl, 5 mM EDTA, 5 mg/ml iodoacetamide, 10 µg/ml PMSF, and the Roche protease inhibitor cocktail). After centrifugation, biotinylated proteins were pulled down with NeutrAvidin beads.

For detection of internalized LRP6 proteins, cells were biotinylated as described above. Then cell surface biotins were stripped with 100 mM MesNa at 4°C for 10 min, followed by free SH groups quenching by 5 mg/ml iodoacetamide. Cells were subsequently lysed, and internalized biotinylated proteins were pulled down with the NeutrAvidin beads.

Online supplemental material
Fig. S1 shows PtdIns(4,5)P_2 contents and the interactions between LRP6 and CHC/AP2. Fig. S2 shows LRP5/6 C-terminal amino acid sequence alignments and internalization assays. Fig. S3 shows STORM analysis of clathrin and LRP6 staining. Online supplemental material is available at http://www.jcb.org/cgi/content/full/jcb.201206096/DC1.

References

Bilic, J., Y.L. Huang, G. Davidson, T. Zimmermann, C.M. Cruciat, M. Bienz, and C. Niehrs. 2007. Wnt induces LRP6 signalosomes and promotes dishevelled-dependent LRP6 phosphorylation. *Science*. 316:1619–1622. http://dx.doi.org/10.1126/science.1137065

Blitzer, J.T., and R. Nusse. 2006. A critical role for endocytosis in Wnt signaling. *BMC Cell Biol*. 7:28. http://dx.doi.org/10.1186/1471-2121-7-28

Boll, W., H. Ohno, Z. Songyang, I. Rapoport, L.C. Cantley, J.S. Bonifacino, and T. Kirchhausen. 1996. Sequence requirements for the recognition of tyrosine-based endocytic signals by clathrin AP-2 complexes. *EMBO J*. 15:5789–5795.

Clevers, H., and R. Nusse. 2012. Wnt/β-catenin signaling and disease. *Cell*. 149:1192–1205. http://dx.doi.org/10.1016/j.cell.2012.05.012

Cruciat, C.M., B. Ohkawara, S.P. Acebron, E. Karaulanov, C. Reinhard, D. Ingelfinger, M. Boutros, and C. Niehrs. 2010. Requirement of prorenin receptor and vacuolar H+-ATPase-mediated acidification for Wnt signaling. *Science*. 327:459–463. http://dx.doi.org/10.1126/science.1179802

Davidson, G., W. Wu, J. Shen, J. Bilic, U. Fenger, P. Stannek, A. Glinka, and C. Niehrs. 2005. Casein kinase 1 gamma couples Wnt receptor activation to cytoplasmic signal transduction. *Nature*. 438:867–872. http://dx.doi.org/10.1038/nature04170

Dempsey, G.T., J.C. Vaughan, K.H. Chen, M. Bates, and X. Zhuang. 2011. Evaluation of fluorophores for optimal performance in localization-based super-resolution imaging. *Nat. Methods*. 8:1027–1036. http://dx.doi.org/10.1038/nmeth.1768

Di Paolo, G., and P. De Camilli. 2006. Phosphoinositides in cell regulation and membrane dynamics. *Nature*. 443:651–657. http://dx.doi.org/10.1038/nature05185

Grumolato, L., G. Liu, P. Mong, R. Mudbhary, R. Biswas, R. Arroyave, S. Vijayakumar, A.N. Economides, and S.A. Aaronson. 2010. Canonical and noncanonical Wnts use a common mechanism to activate completely unrelated coreceptors. *Genes Dev*. 24:2517–2530. http://dx.doi.org/10.1101/gad.1957710

Haucke, V. 2005. Phosphoinositide regulation of clathrin-mediated endocytosis. *Biochem. Soc. Trans*. 33:1285–1289. http://dx.doi.org/10.1042/BST20051285

Huang, B., S.A. Jones, B. Brandenburg, and X. Zhuang. 2008a. Whole-cell 3D STORM reveals interactions between cellular structures with nanometer-scale resolution. *Nat. Methods*. 5:1047–1052. http://dx.doi.org/10.1038/nmeth.1274

Huang, B., W. Wang, M. Bates, and X. Zhuang. 2008b. Three-dimensional super-resolution imaging by stochastic optical reconstruction microscopy. *Science*. 319:810–813. http://dx.doi.org/10.1126/science.1153529

Irie, F., M. Okuno, E.B. Pasquale, and Y. Yamaguchi. 2005. EphrinB-EphB signalling regulates clathrin-mediated endocytosis through tyrosine phosphorylation of synaptojanin 1. *Nat. Cell Biol*. 7:501–509. http://dx.doi.org/10.1038/ncb1252

Jiang, Y., X. He, and P.H. Howe. 2012. Disabled-2 (Dab2) inhibits Wnt/β-catenin signalling by binding LRP6 and promoting its internalization through clathrin. *EMBO J*. 31:2336–2349. http://dx.doi.org/10.1038/emboj.2012.83

Jones, S.A., S.H. Shim, J. He, and X. Zhuang. 2011. Fast, three-dimensional super-resolution imaging of live cells. *Nat. Methods*. 8:499–508. http://dx.doi.org/10.1038/nmeth.1605

Kirchhausen, T. 2009. Imaging endocytic clathrin structures in living cells. *Trends Cell Biol.* 19:596–605. http://dx.doi.org/10.1016/j.tcb.2009.09.002

Krauss, M., and V. Haucke. 2007. Phosphoinositide-metabolizing enzymes at the interface between membrane traffic and cell signalling. *EMBO Rep.* 8:241–246. http://dx.doi.org/10.1038/sj.embor.7400919

Krauss, M., V. Kukhtina, A. Pechstein, and V. Haucke. 2006. Stimulation of phosphatidylinositol kinase type I-mediated phosphatidylinositol (4,5)-bisphosphate synthesis by AP-2mu-cargo complexes. *Proc. Natl. Acad. Sci. USA*. 103:11934–11939. http://dx.doi.org/10.1073/pnas.0510306103

MacDonald, B.T., K. Tamai, and X. He. 2009. Wnt/beta-catenin signaling: components, mechanisms, and diseases. *Dev. Cell*. 17:9–26. http://dx.doi.org/10.1016/j.devcel.2009.06.016

Mao, J., J. Wang, B. Liu, W. Pan, G.H. Farr III, C. Flynn, H. Yuan, S. Takada, D. Kimelman, L. Li, and D. Wu. 2001. Low-density lipoprotein receptor-related protein-5 binds to Axin and regulates the canonical Wnt signaling pathway. *Mol. Cell*. 7:801–809. http://dx.doi.org/10.1016/S1097-2765(01)00224-6

McMahon, H.T., and E. Boucrot. 2011. Molecular mechanism and physiological functions of clathrin-mediated endocytosis. *Nat. Rev. Mol. Cell Biol.* 12:517–533. http://dx.doi.org/10.1038/nrm3151

Nishimura, N., and T. Sasaki. 2008. Cell-surface biotinylation to study endocytosis and recycling of occludin. *Methods Mol. Biol.* 440:89–96. http://dx.doi.org/10.1007/978-1-59745-178-9_7

Nishita, M., S. Itsukushima, A. Nomachi, M. Endo, Z. Wang, D. Inaba, S. Qiao, S. Takada, A. Kikuchi, and Y. Minami. 2010. Ror2/Frizzled complex mediates Wnt5a-induced AP-1 activation by regulating Dishevelled polymerization. *Mol. Cell. Biol.* 30:3610–3619. http://dx.doi.org/10.1128/MCB.00177-10

Ohno, H. 2006. Clathrin-associated adaptor protein complexes. *J. Cell Sci.* 119:3719–3721. http://dx.doi.org/10.1242/jcs.03085

Ohno, H., J. Stewart, M.C. Fournier, H. Bosshart, I. Rhee, S. Miyatake, T. Saito, A. Gallusser, T. Kirchhausen, and J.S. Bonifacino. 1995. Interaction of tyrosine-based sorting signals with clathrin-associated proteins. *Science*. 269:1872–1875. http://dx.doi.org/10.1126/science.7569928

Pan, W., S.C. Choi, H. Wang, Y. Qin, L. Volpicelli-Daley, L. Swan, L. Lucast, C. Khoo, X. Zhang, L. Li, et al. 2008. Wnt3a-mediated formation of phosphatidylinositol 4,5-bisphosphate regulates LRP6 phosphorylation. *Science*. 321:1350–1353. http://dx.doi.org/10.1126/science.1160741

Poccia, D., and B. Larijani. 2009. Phosphatidylinositol metabolism and membrane fusion. *Biochem. J.* 418:233–246. http://dx.doi.org/10.1042/BJ20082105

Rust, M.J., M. Bates, and X. Zhuang. 2006. Sub-diffraction-limit imaging by stochastic optical reconstruction microscopy (STORM). *Nat. Methods*. 3:793–795. http://dx.doi.org/10.1038/nmeth929

Sakane, H., H. Yamamoto, and A. Kikuchi. 2010. LRP6 is internalized by Dkk1 to suppress its phosphorylation in the lipid raft and is recycled for reuse. *J. Cell Sci.* 123:360–368. http://dx.doi.org/10.1242/jcs.058008

Sakane, H., H. Yamamoto, S. Matsumoto, A. Sato, and A. Kikuchi. 2012. Localization of glypican-4 in different membrane microdomains is involved in the regulation of Wnt signaling. *J. Cell Sci.* 125:449–460. http://dx.doi.org/10.1242/jcs.091876

Semënov, M.V., X. Zhang, and X. He. 2008. DKK1 antagonizes Wnt signaling without promotion of LRP6 internalization and degradation. *J. Biol. Chem.* 283:21427–21432. http://dx.doi.org/10.1074/jbc.M800014200

Tanneberger, K., A.S. Pfister, K. Brauburger, J. Schneikert, M.V. Hadjihannas, V. Kriz, G. Schulte, V. Bryja, and J. Behrens. 2011. Amer1/WTX couples Wnt-induced formation of PtdIns(4,5)P2 to LRP6 phosphorylation. *EMBO J.* 30:1433–1443. http://dx.doi.org/10.1038/emboj.2011.28

Varnai, P., B. Thyagarajan, T. Rohacs, and T. Balla. 2006. Rapidly inducible changes in phosphatidylinositol 4,5-bisphosphate levels influence multiple regulatory functions of the lipid in intact living cells. *J. Cell Biol.* 175:377–382. http://dx.doi.org/10.1083/jcb.200607116

Wu, D., and W. Pan. 2010. GSK3: a multifaceted kinase in Wnt signaling. *Trends Biochem. Sci.* 35:161–168. http://dx.doi.org/10.1016/j.tibs.2009.10.002

Yamamoto, H., H. Komekado, and A. Kikuchi. 2006. Caveolin is necessary for Wnt-3a-dependent internalization of LRP6 and accumulation of beta-catenin. *Dev. Cell*. 11:213–223. http://dx.doi.org/10.1016/j.devcel.2006.07.003

Yu, A., J.F. Rual, K. Tamai, Y. Harada, M. Vidal, X. He, and T. Kirchhausen. 2007. Association of Dishevelled with the clathrin AP-2 adaptor is required for Frizzled endocytosis and planar cell polarity signaling. *Dev. Cell*. 12:129–141. http://dx.doi.org/10.1016/j.devcel.2006.10.015

Yu, A., Y. Xing, S.C. Harrison, and T. Kirchhausen. 2010. Structural analysis of the interaction between Dishevelled2 and clathrin AP-2 adaptor, a critical step in noncanonical Wnt signaling. *Structure*. 18:1311–1320. http://dx.doi.org/10.1016/j.str.2010.07.010